Expanded View Figures

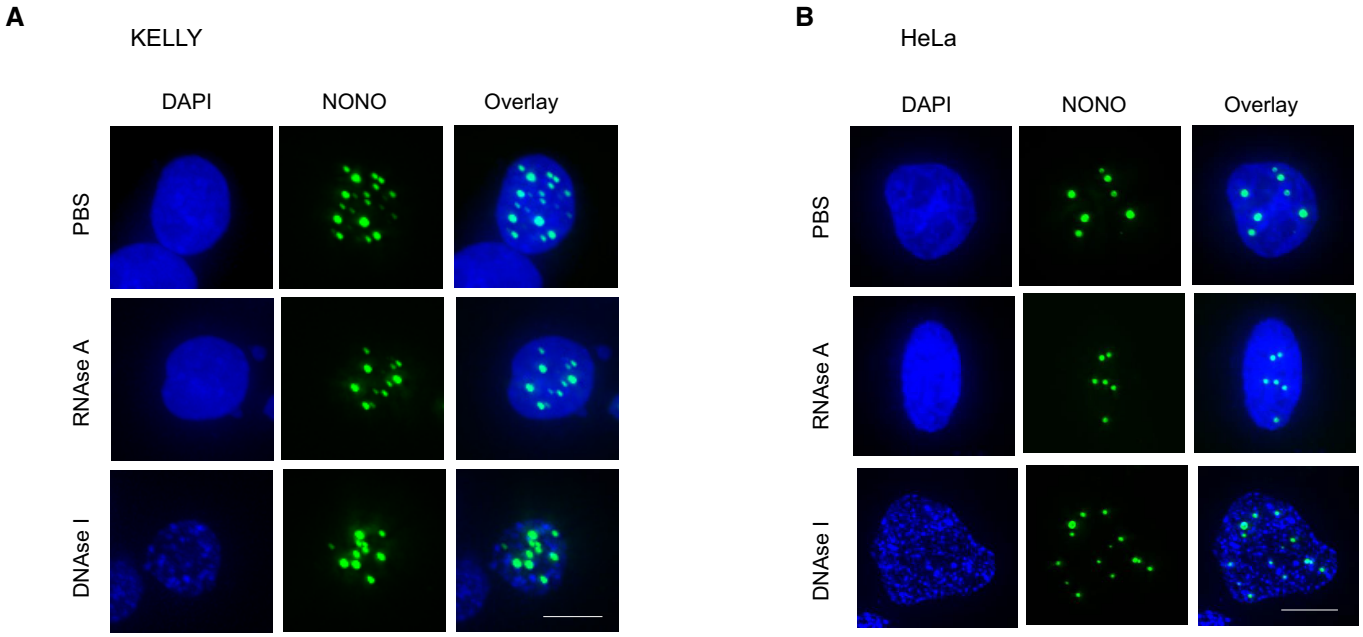

Figure EV1. NONO_ΔRRM1 puncta are resistant to nuclease digestion.

A Fluorescence micrograph images of representative cells stained for NONO in KELLY cells transfected with YFP-NONO_ΔRRM1 and then treated with PBS, RNase A or DNase I, as indicated.

B Fluorescence micrograph images of representative cells for NONO signal in HeLa cells transfected with YFP-NONO_ΔRRM1 and then treated with PBS, RNase A or DNase I.

Data information: Scale bar: 5 μm.

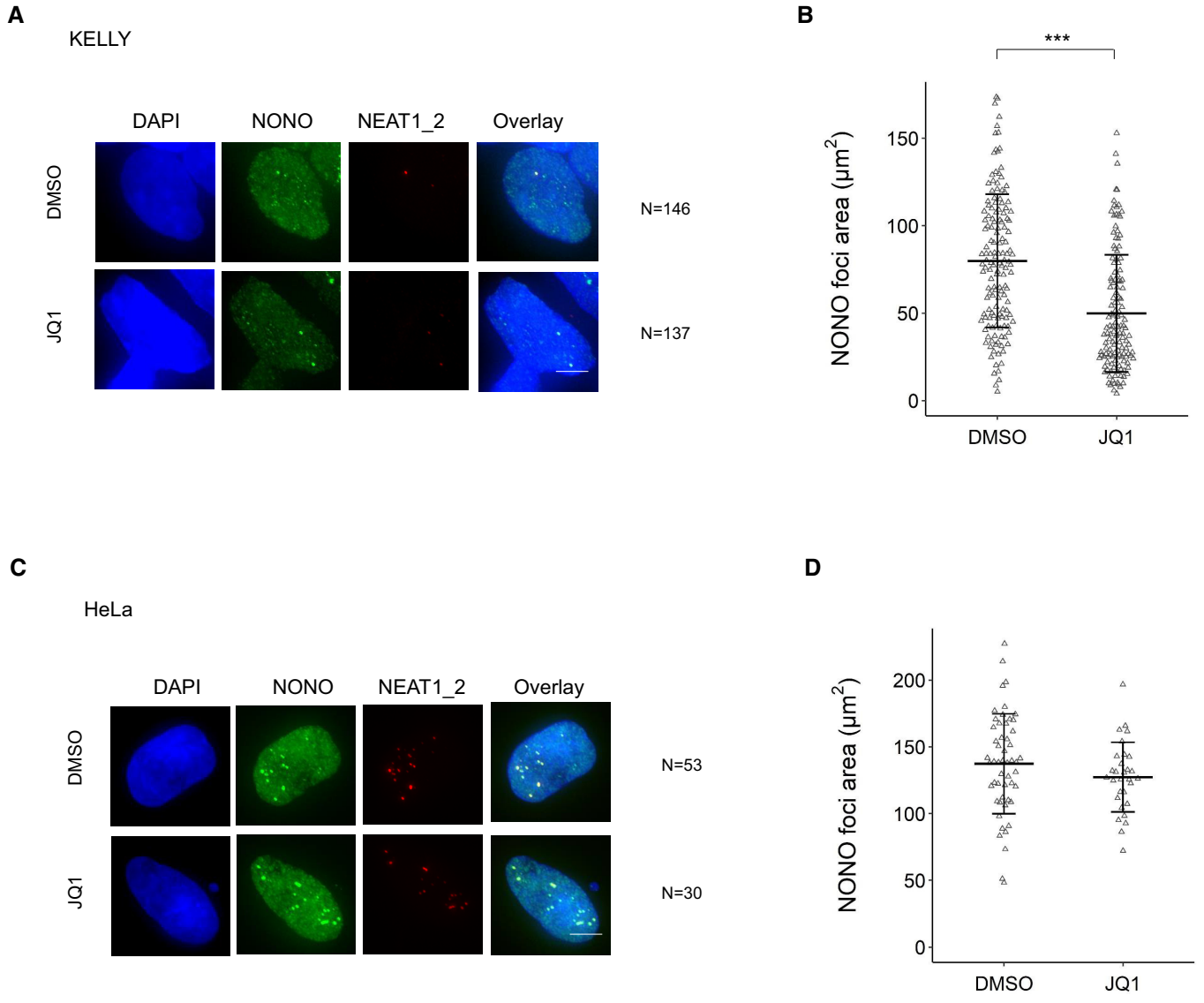

Figure EV2. JQ1 diminishes NONO foci formation in KELLY cells.

A Representative Fluorescence micrograph images of cells stained for NONO and NEAT1_2 in KELLY cells treated with BET inhibitor JQ1. DAPI (blue) stain indicates cell nuclei, NONO immunofluorescence (green) and NEAT1_2 RNA FISH (red). Scale bar: 5 μm.

B Dot plot of NONO foci area (μm^2) per nucleus calculated using images of hundreds of cells, stained as in (A). Bars are SD. The numbers of biological replicates are indicated in (A). Student's *t*-test is used to compare the means. ***$P < 0.001$.

C Representative Fluorescence micrograph images of cells stained for NONO and NEAT1_2 in HeLa cells treated with BET inhibitor JQ1. Scale bar: 5 μm.

D Dot plot of NONO foci area (μm^2) per nucleus calculated using images of cells, stained as in (C). Bars are SD. The numbers of biological replicates are indicated in (C). Student's *t*-test is used to compare the means.

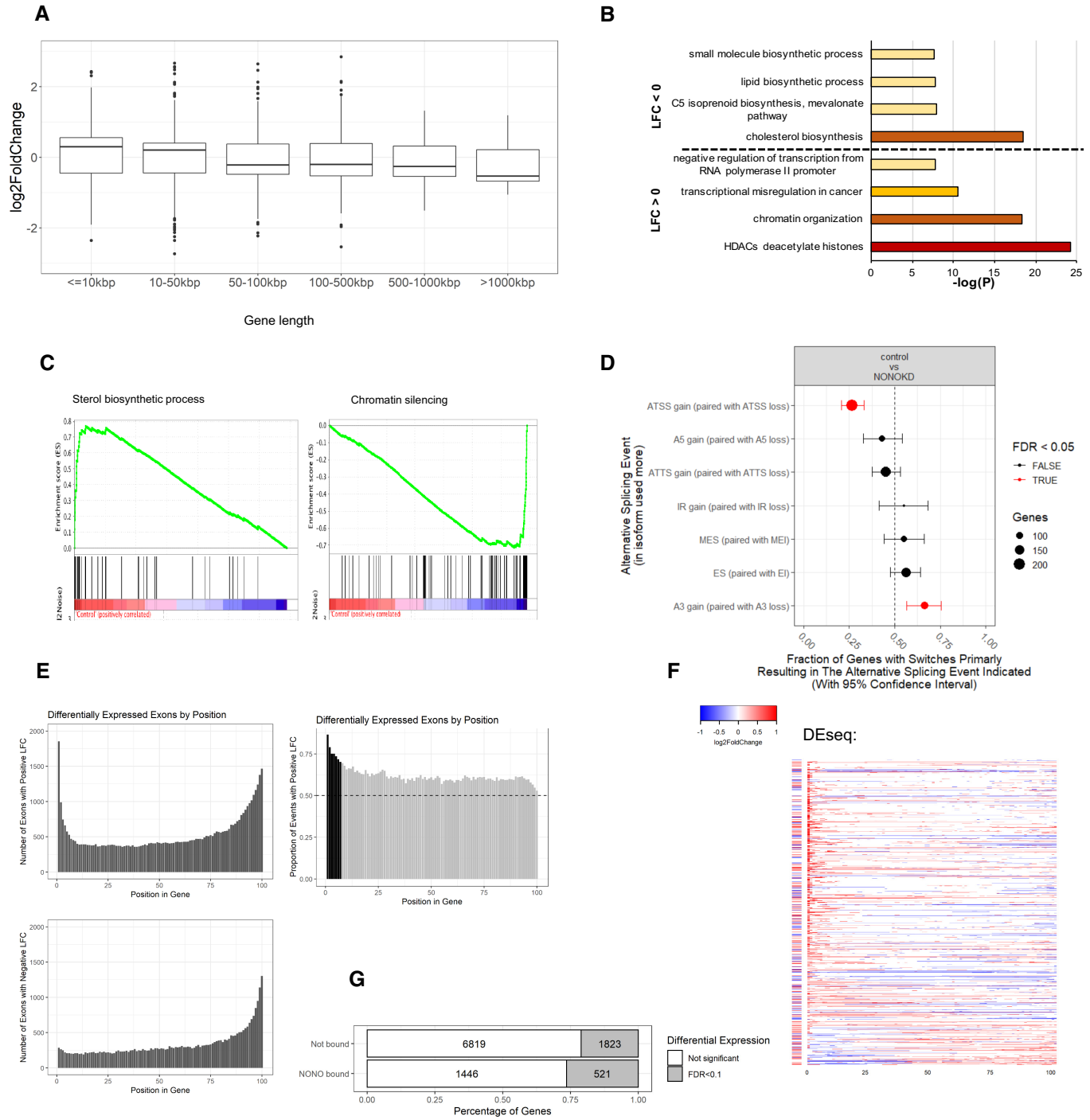

Figure EV3.

Figure EV3. NONO KD induces significant changes in ATSS and A3 in KELLY cells.

A Box plots showing log fold change for genes which were significantly differentially expressed (Padj < 0.1), separated by gene length. Biological replicates $n = 4$ in controls and $n = 8$ in NONO KD samples. Central band is median; boxes represent 1st and 3rd quartile (25th and 75th percentile, respectively) and whiskers 1.5× interquartile range. The numbers of genes are 948, 1,466, 534, 584, 48 and 14 for gene length ≤ 10, 10–50, 50–100, 100–500, 500–1,000 and > 1,000 kbp, respectively. (B) Summary of most highly enriched gene ontology categories produced by "Metascape" analysis of significantly upregulated (LFC > 0) and downregulated (LFC < 0) genes following NONO KD.

B Enrichment score profile plots produced by "GSEA" for the "sterol biosynthetic process" and "chromatin silencing" gene sets, respectively.

C NONO KD results in significant splicing events including ATSS and A3. The error bars represent 95% confidence intervals. Biological replicates $n = 4$ in controls and $n = 8$ in NONO KD samples.

D Top panel is a histogram of numbers of exons with significant positive differential expression events in NONO KD compared to control, ranked by gene position. Bottom panel is the same analysis, but for numbers of exons with negative differential expression events. Right panel shows the proportion of positive differential expression events, ranked by gene position. The dotted line at 0.5 indicates equal numbers of positive, and negative expression events. The black bars show where positive expression events are significantly occurring, over negative events (> 2 SD over the median).

E Individual transcripts with significant positive, or negative, differential expression exons at the 5′ end of the gene (bins 1–7 from Fig EV3E). Each row represents a gene, split into 100 bins (exons and introns). Coloured bins represent significant events in differential expression. The bar to the left of each row indicates whether the gene as a whole is differentially expressed. Red indicates increased expression, and blue indicates decreased expression.

F Proportions of differentially expressed genes between NONO-bound and non-bound target genes.

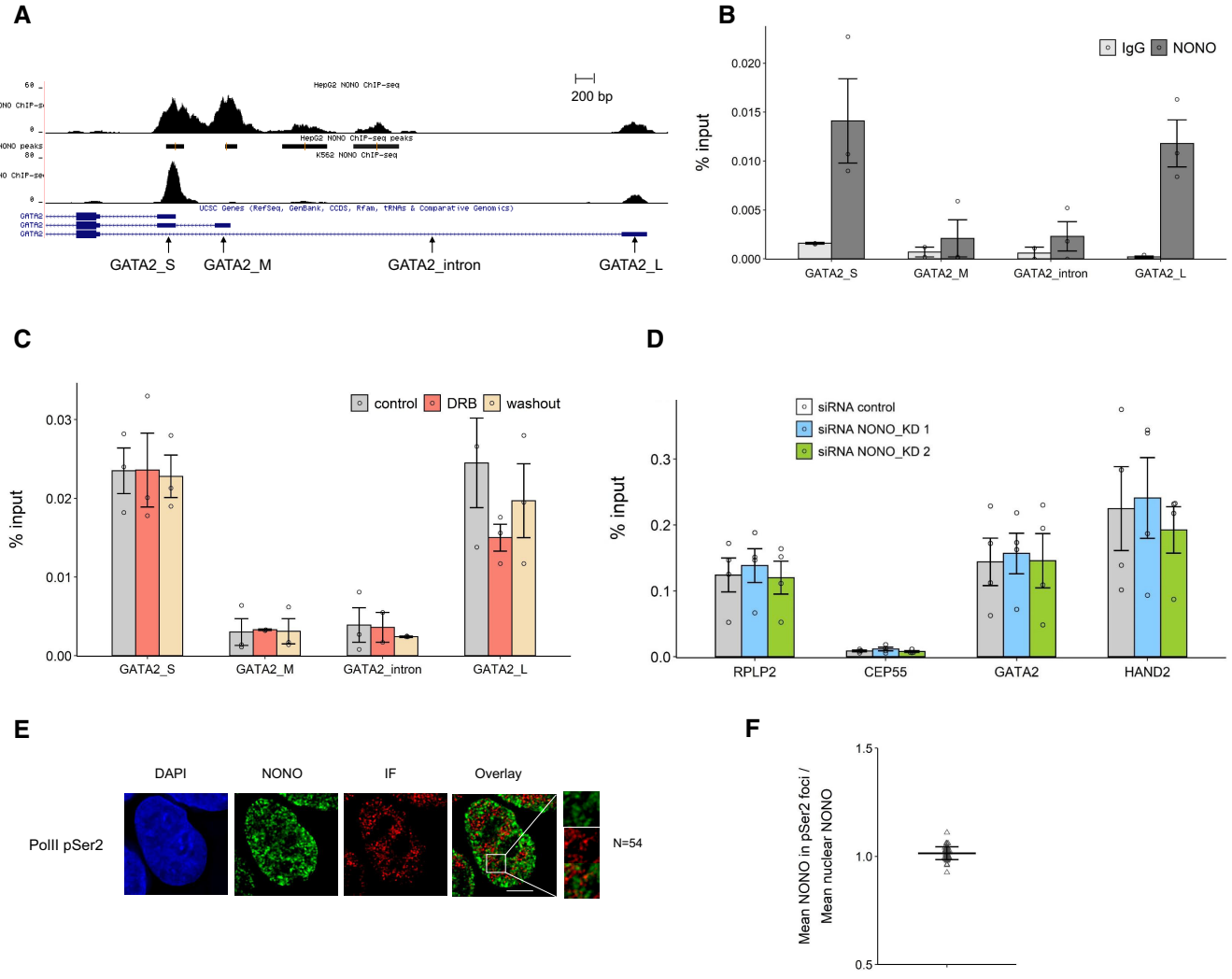

Figure EV4.

Figure EV4. NONO displays some DNA binding to GATA2, which in turn is not sensitive to transcription levels, or linked to transcriptional elongation.

A NONO ChIP-seq peaks for GATA2 in HepG2 and K562 cell lines shown as a Genome Browser image (Xiao *et al*, 2019). The primer pairs for GATA2 used in our ChIP-qPCR are indicated.
B The enrichment of relative GATA2 chromatin fragments via ChIP-qPCR against NONO and normal mouse serum IgG in KELLY cells. Bars are SEM. Biological replicates $n = 3$.
C NONO ChIP-qPCR indicates the enrichment of relative GATA2 chromatin fragments in KELLY cells treated with control, DRB and DRB followed by a washout period. Bars are SEM. Biological replicates $n = 3$.
D The enrichment of relative GATA2 and HAND2 chromatin fragments after NONO KD via ChIP-qPCR against RNA PolII phosphorated at Serine 2 in KELLY cells. Bars are SEM. Biological replicates $n \geq 3$.
E Fluorescence micrograph images of representative cells stained for NONO and RNA PolII phosphorated at Serine 2. DAPI (blue) stain indicates cell nuclei, NONO immunofluorescence (green) and immunofluorescence for Pol II pSer2 (red). Scale bar: 5 μm.
F In micrograph image quantitation analysis, the enrichment of mean NONO fluorescence detected within immunofluorescence foci of Pol II pSer2 is determined as a ratio relative to mean nuclear NONO fluorescence in (E). The quantitation shows no enrichment of NONO in the foci. Bars are SD. Biological replicates $n = 54$.

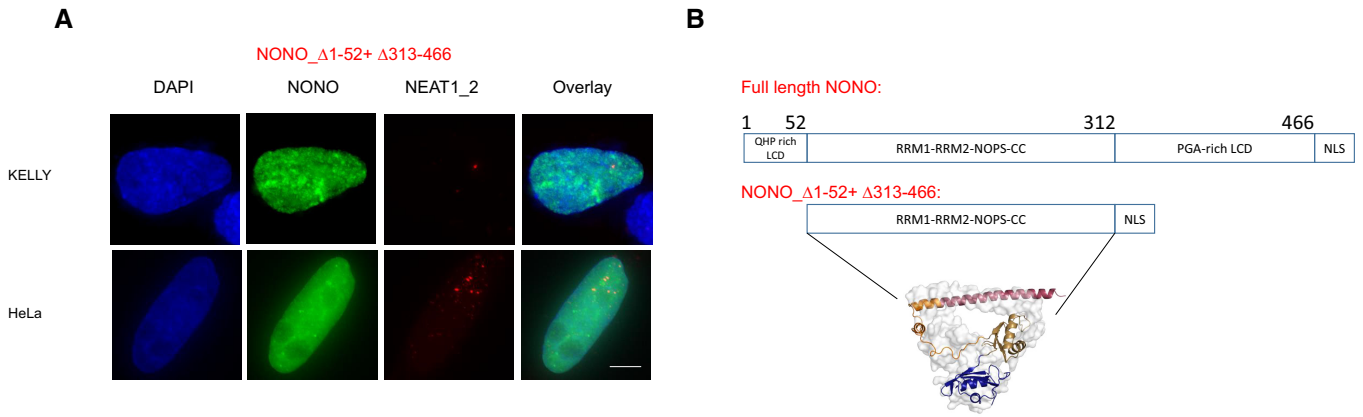

Figure EV5. NONO construct lacking the N- and C-terminal low complexity domain is more diffuse in the nucleus than wildtype NONO.

A Fluorescence micrograph images of representative cells stained for NONO and NEAT1_2 in KELLY and HeLa cells transfected with GFP fused NONO_Δ1–52 + Δ313–466 plasmids. Scale bar: 5 μm.
B Construction of NONO_Δ1–52 + Δ313–466 plasmids, indicating how the mutant lacking the N- and C-terminal LCD is equivalent to a soluble structured dimer, previously solved by crystallography (PDB 3SDE).